ACS APPLIED MATERIALS & INTERFACES

Research Article

www.acsami.org

# Protein–Gold Hybrid Nanocubes for Cell Imaging and Drug Delivery

Han Ding,[†] Dongying Yang,[‡] Chen Zhao,[§] Zhuokun Song,[∥] Pengchang Liu,[†,⊥] Yu Wang,[§] Zhijun Chen,*[,†,⊥] and Jiacong Shen[†]

[†]State Key Laboratory of Supramolecular Structure and Materials, Jilin University, 2699 Qianjin Street, 130012 Changchun, People's Republic of China

[‡]Department of Chemistry, Fudan University, 220 Handan Road, Yangpu District, 200433 Shanghai, People's Republic of China

[§]State Key Laboratory of Reproductive Biology, Institute of Zoology, Chinese Academy of Sciences, 100101 Beijing, People's Republic of China

[∥]Department of Electrical and Computer Engineering, National University of Singapore, Engineering Drive 3, 117583 Singapore

[⊥]Institute of Theoretical Chemistry, Jilin University, 130012 Changchun, People's Republic of China

Supporting Information

**ABSTRACT:** Multifunctional biocompatible nanomaterials containing both fluorescent and vehicle functions are highly favored in bioimaging, therapeutic, and drug delivery applications. Nevertheless, the rational design and synthesis of highly biocompatible multifunctional materials remain challenging. We present here the development of novel protein–gold hybrid nanocubes (PGHNs), which were assembled using gold nanoclusters, bovine serum albumin, and tryptophan as building blocks. The green-synthesized PGHNs in this study are blue-emitting under UV exposure and cube-shaped with a size of approximately 100 nm. These hybrid nanomaterials are highly biocompatible as shown by cytotoxicity experiments and can be readily internalized by different types of cells. Moreover, PGHNs can act as nanovehicles that successfully deliver dyes or drugs into the cells. The protein–metal hybrid nanocubes can serve as a new type of dual-purpose tool: a blue-emitting cell marker in bioimaging investigation and a nanocarrier in drug delivery studies.

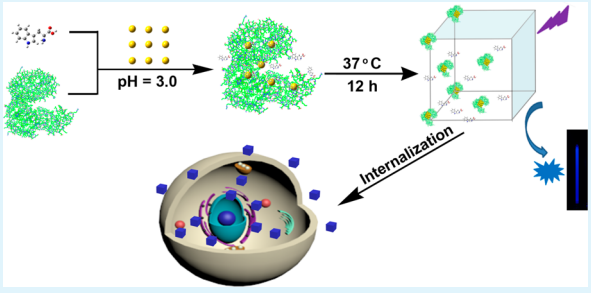


**KEYWORDS:** *protein–gold hybrid nanocubes, blue emission, cell imaging, nanovehicle, drug delivery*

## INTRODUCTION

Bioimaging, as a state-of-the-art technology, is one of the frontiers in biological sciences and has a significant impact in clinical and medical research. It provides visual information for cell condition and disease analysis.[1,2] In recent years nanomaterials such as inorganic quantum dots (Q-dots),[3−6] alongside green fluorescent proteins (GFPs) and organic light-emitting materials,[7−9] have been used as fluorescent markers in sophisticated imaging studies due to their special photophysical properties.[10,11] However, several weak points such as high toxicity and limited options for emission wavelengths of these fluorescent nanomaterials greatly restricted their use in broader areas.[12−16]

As alternatives to Q-dots and fluorescent organic molecules, recently, noble-metal nanoparticles (NPs) and/or nanoclusters (NCs) have attracted much attention because of their unique photoelectrical properties.[17−24] Especially ultrasmall gold, silver, and platinum NCs have been used as fluorescent labels in bioimaging and sensors for the detection of certain target molecules in analytical investigation.[25−29] Notably, during noble-metal NC synthesis, certain toxic or environmentally unfriendly organic molecules such as sodium borohydride, lithium aluminum hydride, hydrazine hydrate, and hydroxylamine hydrochloride are frequently used as reducing or protecting agents.[30,31] Lately, proteins, DNA, and various other biomolecules have also been used in fluorescent NP/NC synthesis, aiming to overcome biocompatibility-related problems.[17−19,32−36] However, there is still much room to improve these fluorescent noble-metal NCs. For instance, most metal NCs reported so far show a low light-emitting efficiency, limited choices in excitation wavelengths, and difficulty being internalized by cells (Table S1, Supporting Information). Moreover, although various nanovehicles such as mesoporous silica nanoparticles (MSNs) are widely used in drug delivery studies,[37] new biocompatible nanomaterials with unique fluorescent emission as well as excellent cell internalization properties are highly desired in bioimaging and drug delivery studies.[38]

In this paper we describe the development of a facile and green method for the synthesis and assembly of novel protein–gold hybrid nanocubes (PGHNs) consisting of gold nanoclusters (AuNCs), bovine serum albumin (BSA), and

Received: November 28, 2014
Accepted: February 11, 2015
Published: February 11, 2015

  

DOI: 10.1021/am5083733
ACS Appl. Mater. Interfaces 2015, 7, 4713−4719

tryptophan (Trp). PGHNs are blue-emitting under UV irradiation and cubelike in overall structure with a size of approximately 100 nm. The whole synthetic process is eco-friendly and toxicity-free, which ensures a high level of compatibility. PGHNs can be readily internalized by different type of cells, which suggests a high efficiency of endocytosis of this material. Moreover, PGHNs can function as nanovehicles that can deliver dyes and drugs into the cells. The protein−metal hybrid nanomaterial can serve as a dual-purpose tool: a blue-emitting cell marker in bioimaging investigation as well as a nanovehicle for drug delivery studies.

## EXPERIMENTAL SECTION

**Chemicals.** Chemical compounds such as sodium hydroxide (NaOH), hydrochloric acid (HCl), phosphate buffer, sodium chloride (NaCl), Tris base, glucose, sucrose, and HEPES were purchased from the Beijing Chemical Reagent Co. (Beijing, China). Double-distilled water ($dH_2O$) used throughout the experiments was produced by a Milli-Q system (Millipore, Bedford, MA). BSA, Trp, and sorbitol were ordered from DingGuoChangsheng Biotechnology Co., Ltd. (Beijing, China). Chloroauric acid ($HAuCl_4$) was obtained from Sinopharm Chemical Reagent Co., Ltd. (Shanghai, China).

**Instruments and Characterization.** Shaker incubation was carried out on an incubator shaker (IS-RDS3, Crystal, Suzhou, China). Centrifuge experiments were carried out with a high-speed refrigerated centrifuge (Anhui USTC Shaker Zonkia Scientific Instruments, Hefei, China). UV−vis spectra were obtained on a UV-3600 spectrophotometer (Shimadzu, Tokyo, Japan, www.shimadzu.com). Fluorescence spectra were obtained on a 5301PC spectrophotometer (Shimadzu, Toko, Japan, www.shimadzu.com). The fluorescence lifetimes of the samples were recorded on an Edinburgh Instruments fls920 spectrofluorometer equipped with a continuous (450 W) xenon lamp (Edinburgh, U.K., www.edinst.com). For size and morphology analysis, field emission transmission electron microscopy (TEM) images were acquired on a JEM-2100F transmission electron microscope (Tokyo, Japan). Atomic force microscopy (AFM) images were collected on an SPA 300 atomic force microscope (NSK, Japan). Scanning electron microscopy (SEM) images were acquired on an XL 30 ESEM FEG scanning electron microscope (FEI, United States). X-ray photoelectron spectroscopy (XPS) data were collected on a Kratos AXIS X-ray photoelectron spectrometer (Manchester, UK, www. Kratos.com). The Malvern ZEN 3600 zetasizer (Malvern Instruments Ltd., United Kingdom) was used to investigate the synthesized particle size and $\zeta$ potential. Microbe fluorescent images were collected using a laser confocal inverted microscope (FV1000, Olympus, Japan).

**Synthesis of PGHNs.** All glassware used in the reaction process was soaked in aqua regia and then washed and dried. PGHNs were synthesized at 37 °C and pH 3.0 in the presence of Trp and BSA (Scheme 1). Briefly, Trp, BSA, and chloroauric acid were added to a $dH_2O$ solution to final concentrations of 20, 5, and 1.6 mg/mL, respectively. The mixture was immediately adjusted to pH 3.0 and then incubated at 37 °C for 12 h. In addition, we also tested different synthesis conditions by changing the pH, stabilizers, and so on. The synthesized PGHNs were dialyzed against $dH_2O$ and stored at 4 °C. Calculation of the concentration of PGHNs was based on an assumption that all the $Au^{3+}$ ions during the synthesis of PGHNs were reduced to form AuNCs. For instance, 0.2 mM PGHNs means that the concentration of the sum of $Au^+$ and $Au^0$ atoms within the solution was 0.2 mM. In addition, the method used for PGHN quantum yield (QY) measurement set rhodamine 6G (Rh 6G) as the reference standard. The QY of PGHNs was calculated on the basis of the formula QY = X1/X2 × 95, where X1 and X2 refer to the average integral of the fluorescence emission of PGHNs and Rh 6G, respectively.

**Cell Culture and Imaging.** For *Escherichia coli*/*Saccharomyces cerevisiae* imaging, cells were incubated to logarithmic phase ($OD_{600}$ = 0.5/5.0). These microbes were collected by using a centrifuge and resuspended in fresh LB/YPD medium. PGHNs were then added to the medium at a concentration of 0.2 mM followed by rotation incubation for 6 h at room temperature. The cells were washed three times using PBS buffer (pH 7.4) and then subjected to imaging analysis.

**Scheme 1. Schematic Presentation of PGHN Synthesis and Their Application in Cell Imaging and Drug Delivery Studies**[a]

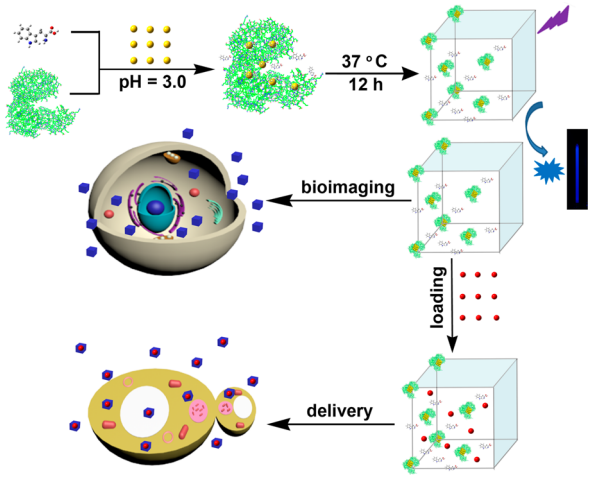


[a]The yellow dot, the blue cube, and the red circle stand for AuNCs, PGHNs, and Rh 6G (or Dox), respectively.

Human embryonic kidney (HEK) 293 cells were maintained in DMEM medium supplemented with 10% (v/v) fetal bovine serum (FBS), 100 U/mL penicillin, and 100 mg/mL streptomycin. Approximately $5 \times 10^4$ cells were seeded into each well in a 24-well plate and incubated overnight at 37 °C with 5% $CO_2$ in a humidified atmosphere. The next day, the culture medium was replaced by 200 $\mu$L of medium containing PGHNs (0.2 mM). Cellular uptake was detected by a high-content imaging fluorescent microscope (Operetta from PerkinElmer) after 6 h of incubation at 37 °C and washing with PBS buffer (pH 7.4) twice. A fixed excitation wavelength of 405 nm was used for all the confocal fluorescent microscopy (CFM) experiments. The emission wavelengths used for the CFM analysis were 480 (for PGHNs) and 610 nm (for doxorubicin (Dox) and Rh 6G).

**Cytotoxicity Analysis.** The cytotoxicity of PGHNs was evaluated using *E. coli* as a model system. The *E. coli* DH5$\alpha$ colony was picked up from the LB plate and incubated overnight (12 h) at 37 °C (150 rpm) until $OD_{600}$ of the culture reached approximately 3.5. Bacteria cells were harvested by centrifugation, washed three times using PBS buffer (pH 7.4), and resuspended with fresh LB medium to $OD_{600}$ = 0.3. The cells were divided into two groups: one group was mixed with PGHNs, and the other was mixed with an equal volume of PBS buffer serving as a control. These samples were further incubated at 37 °C (150 rpm by shaking) until the cells reached a steady growth ($OD_{600}$ was measured at intervals).

**Loading of Dye and/or Drug Molecules.** Rh 6G (0.1 mg/mL) or Dox (0.1 mg/mL) was mixed with PGHNs (0.2 mM) containing neutralized aqueous solution and the resulting stirred for 12 h in a dark place. The mixture was then dialyzed against $dH_2O$ to remove unbound Rh 6G or Dox until no fluorescent signal could be detected from the solutions outside of the dialysis tubes.

For the drug release test, PGHN−Rh 6G (400 $\mu$L) was added to the dialysis bag and incubated with 3 mL buffer solutions (either 1 × PBS buffer, pH 7.4, or 20 mM HAc−NaAc buffer, pH 4.7) in a cuvette. The release of Rh 6G toward the buffer solutions was monitored by using UV−vis absorption spectra (at 530 nm).


DOI: 10.1021/am5083733
ACS Appl. Mater. Interfaces 2015, 7, 4713−4719

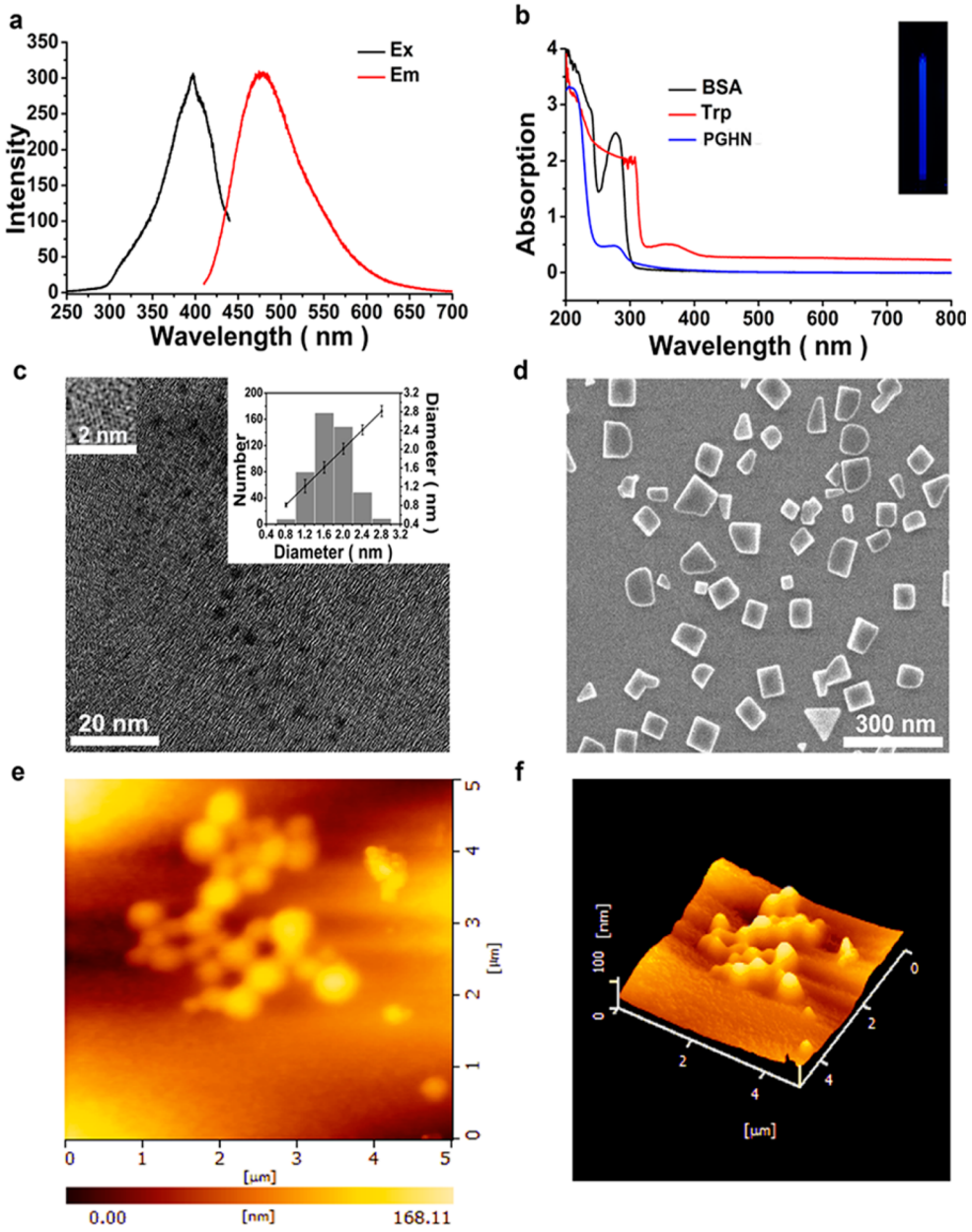


**Figure 1.** Fluorescence, UV−vis, TEM, SEM, and AFM characterization of PGHNs. (a) The excitation and emission peaks of PGHNs are localized at 395 and 480 nm, respectively. (b) UV−vis spectra of BSA, Trp, and PGHN. The inset image shows the blue emission of PGHNs under UV irradiation (365 nm). (c) Representative TEM image of AuNCs within PGHNs. The average size of the gold core of these AuNCs is 1.8 ± 0.4 nm. (d) SEM image showing the nanocube assembly of PGHNs. The average size of the nanocubes is approximately 100 nm. Images e and f show the representative 2D and 3D morphologies of PGHNs.

## RESULTS AND DISCUSSION

Inspired by studies concerning protein-assisted synthesis of AuNCs, we reasoned that the combination of the building blocks of proteins, namely, certain amino acids and other capping agents, might be a convenient way to synthesize fluorescent hybrid materials. Among 20 natural amino acids, Trp is regularly used in the synthesis of noble-metal NPs.[39−49] Concerning Trp-assisted synthesis of NPs, however, most of the reported Trp-conjugated NPs are either nonfluorescent or large in size (Table S2, Supporting Information). A series of experiments have been carried out to evaluate the possibility of a combination approach by using Trp to synthesize new fluorescent nanomaterials in the presence of eco-friendly molecules such as BSA, DNA, glutathione, glucose, sorbitol, chloramphenicol, or other nontoxic or low-toxicity molecules (Figure S1, Supporting Information). It was shown that Trp plus BSA was an excellent combination for the synthesis of fluorescent PGHNs (Figures S2−S6, Supporting Information). The synthetic condition of PGHNs was carefully analyzed and optimized (Figures S7 and S8, Supporting Information).

The excitation and emission of PGHNs are centered at 395 and 480 nm, respectively (Figure 1a). Compared to previously reported BSA-conjugated red-emitting AuNCs (BSA−AuNCs),[17] the shifted emission wavelength of PGHNs might be associated with the density and type of surface ligands of the gold cores.[50] Notably, the excitation at 395 nm approaches the first laser irradiation wavelength (405 nm) of fluorescent microscopy, hinting that PGHNs may be a candidate in


DOI: 10.1021/am5083733
ACS Appl. Mater. Interfaces 2015, 7, 4713−4719

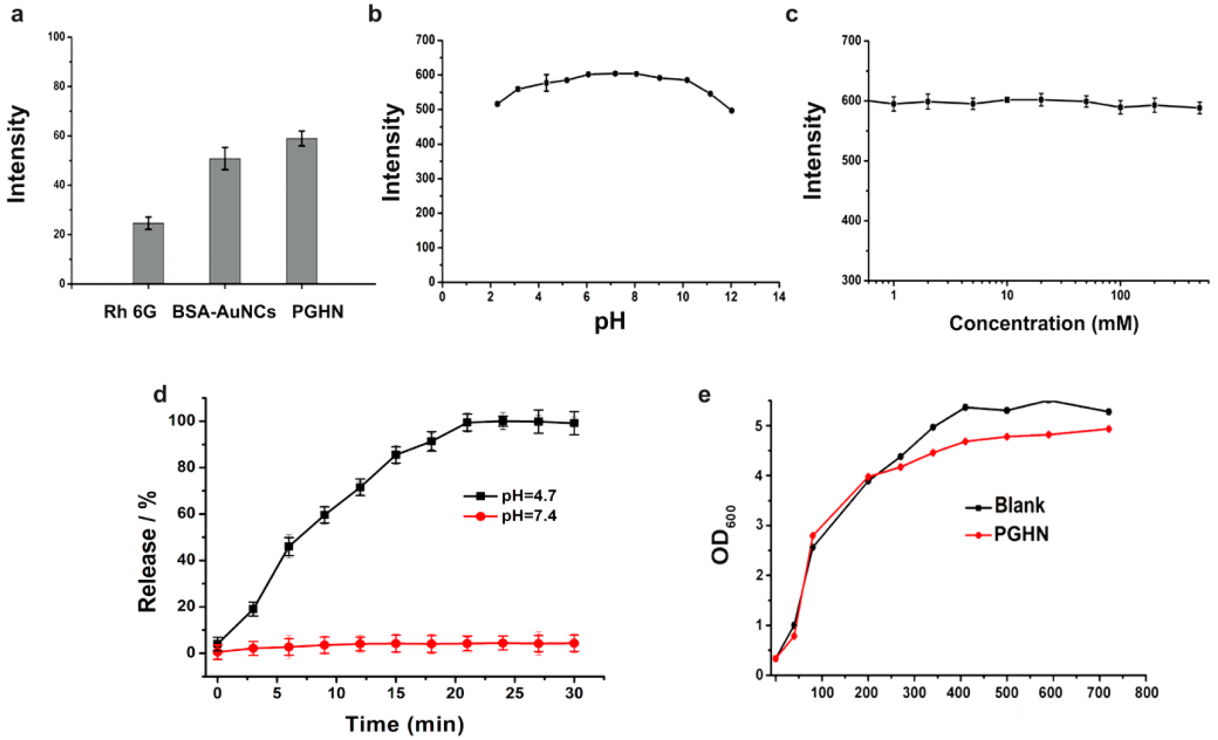


**Figure 2.** Photostability, drug release behavior, and cytotoxicity of PGHNs. (a) Fluorescence photobleaching experiment showing that PGHNs are resistant to irradiation (355 nm laser at 3.5 mW for 5 min) as compared to Rh 6G and BSA−AuNCs. (b) pH stability of PGHNs as indicated by the fluorescence intensity at 480 nm. (c) Photostability of PGHNs at different salt concentrations (NaCl). (d) Drug release profile of PGHNs at different pH conditions. (e) Cytotoxicity of PGHNs evaluated using *E. coli* as a model. As shown on the growth curve, PGHN did not show a clear observable toxic effect toward *E. coli* cells. The optical density (OD) measurement was fixed at 600 nm. The values are plotted as the mean ± SD ($n$ = 3).

bioimaging studies (Scheme 1). Like most proteins, both BSA and Trp showed a strong peak primarily localized at 280 nm as shown by UV−vis absorption spectra. This protein characteristic peak was diminished when PGHNs were formed (Figure 1b), which likely resulted from the light-absorbing characteristic of the synthesized AuNPs/NCs. The fluorescence lifetime of PGHNs was 4.74 ns (Figure S9, Supporting Information), which is similar to those of most of the reported fluorescent AuNCs.[17−19,32−36]

The quantum yield of PGHNs was 7.13% using rhodamine 6G as a reference, which is among the highest within the reported fluorescent gold NPs/NCs, especially for those capped with biocompatible agents (Table S1, Supporting Information). XPS showed two binding peaks present at 84.4 eV ($4f_{7/2}$) and 87.2 eV ($4f_{5/2}$) (Figure S10, Supporting Information), which suggests that the gold core of the PGHN assembly was formed by $Au^0$ and $Au^+$.[17,51−53] The binding energy of $4f_{7/2}$ can be further divided into 84.4 and 87.2 eV, and thus, the contents of $Au^0$ and $Au^+$ can be deduced to be 75.64% and 24.36%, respectively. TEM showed that the gold core of AuNCs within the PGHN assembly had a round shape with an average size of approximately 1.8 nm (Figure 1c).

These small-sized NCs were assembled into higher supramolecular structures (PGHNs) approximately 100 nm in size (Figure 1d−f; Figure S12, Supporting Information). The assembly mechanism of the cubelike supramolecular structure is currently unclear. Nevertheless, we speculate that this assembly might be similar to protein crystal formation where Trp and/or AuNCs play a role in stabilizing the structure. The possible cross-linking event between BSA/Trp that coats AuNCs may fix the cubelike structure (unpublished data).[18,19] The detailed mechanism of the putative crystal-like and cross-link-facilitated PGHN assembly is currently under investigation in our laboratory. The surfaces of these supramolecuar structures are slightly negatively charged (Figure S13, Supporting Information). PGHNs resisted photobleaching (Figure S16, Supporting Information) and exhibited excellent photostability toward the change of pH (Figure S17, Supporting Information) and salt concentration (Figure S18, Supporting Information), suggesting a probability of this material as a new fluorescent marker.

The cytotoxicity of PGHNs was evaluated by using *E. coli* bacteria cells as a model system. PGHNs showed low toxicity toward the bacteria cells at least up to 0.2 mM (Figure 2), which suggests that this material may be suitable for in vivo or ex vivo studies.

The size, shape, surface, and other properties of PGHNs suggest a possibility of this material serving as a fluorescent marker for bioimaging and a nanovehicle for drug delivery. The fluorescence and internalization properties of PGHNs were investigated using bacteria (*E. coli*), yeast (*S. cerevisiae*), and mammalian cells (HEK 293 cells). These cells were incubated with PGHNs (0.2 mM) at room temperature for 6 h and washed multiple times using phosphate-buffered solution (PBS buffer, pH 7.4). The cells were imaged using a confocal fluorescence microscope. Interestingly, PGHNs can be easily internalized by *E. coli*, *S. cerevisiae*, and HEK 293 cells, as shown by the strong blue-emitting signals within the cytoplasm of these cells (Figure 3), whereas several other fluorescent AuNCs synthesized by using other approaches were not (data not


DOI: 10.1021/am5083733
*ACS Appl. Mater. Interfaces* 2015, 7, 4713−4719

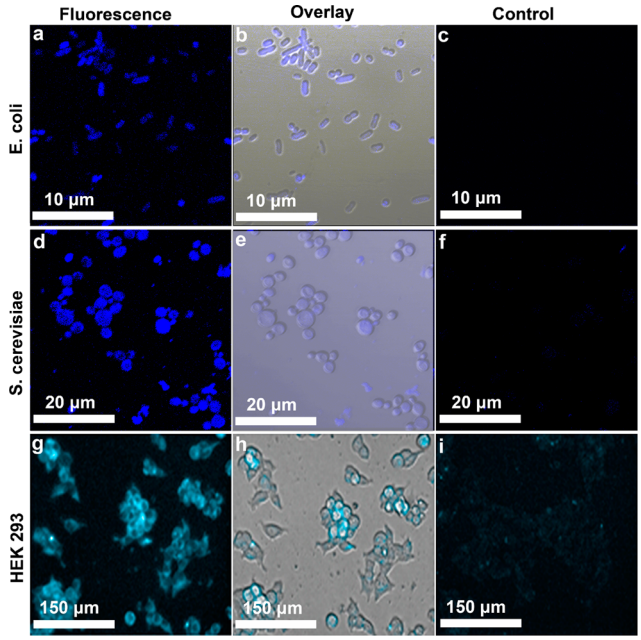


**Figure 3.** PGHNs can be internalized by bacteria, yeast, and mammalian cells likely through endocytosis. Confocal fluorescent micrographs show that PGHNs entered *E. coli*, *S. cerevisiae*, and HEK 293 cells and emitted blue signals upon UV irradiation. The fluorescence images were collected with excitation at 405 nm (a, d, g). The overlaid images (b, e, h) are the merged pictures of fluorescent and bright field images. Images c, f, and i are for cells without incubation with PGHNs, which serve as controls.

shown). Taken together, PGHNs can be an excellent fluorescent cell marker for bacteria, fungi, and mammalian cells.

To test the capability of PGHNs in serving as a vehicle for drug delivery, Rh 6G and Dox were loaded onto PGHNs separately on the basis of the electrostatic interaction between PGHNs and these small molecules. Under neutral pH conditions, the surface charges of PGHNs, Rh 6G, and Dox are approximately −28, 14, and 15 mV, respectively (Figure S13−S15, Supporting Information). *S. cerevisiae* cells were incubated with PGHN−Rh 6G and/or PGHN−Dox for 6 h and then washed multiple times by using PBS buffer (pH 7.4) based on a centrifugation system until no fluorescent signal could be detected from the supernatant. The cells were dissected by using CFM. Similar to the cell imaging study shown in Figure 3d, PGHN−Rh 6G can be internalized by *S. cerevisiae* cells and showed evenly distributed fluorescent blue (from PGHNs) and red (from Rh 6G) signals when they were laser irradiated at different wavelengths (Figure 4a−d). PGHN−Dox can also be efficiently taken up by these yeast cells (Figure 4e−h). Nevertheless, Dox showed a punctuated pattern (Figure 4f) which was different from that of PGHNs, suggesting Dox can be released from the PGHN−Dox complex within cells and enter the nucleus. This observation was in accordance with previous Dox-related drug delivery reports where Dox diffused from the cytosol to the nucleus and interacted with DNA by intercalation.[54,55] These results suggest that PGHNs can deliver drugs into the eukaryotic cells and unload them at the cytoplasm, while the final destinations of the drugs partially depend on their biochemical properties. It would be interesting to generate the upgraded version of PHGNs, which could transport the drugs to specific organelles within the eukaryotic cells.

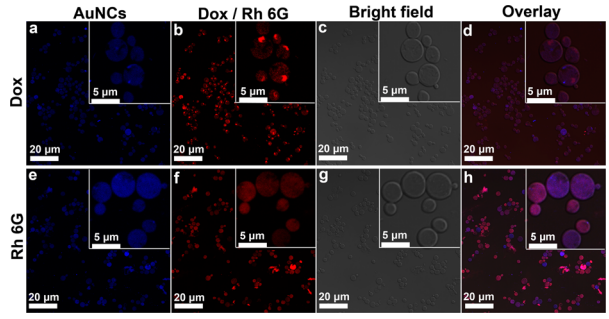


**Figure 4.** PGHN−Rh 6G and PGHN−Dox can be efficiently internalized by *S. cerevisiae* cells. CFM micrographs showed evenly distributed patterns of PGHNs (a) and Rh 6G (b) within *S. cerevisiae* cells when PGHN−Rh 6G was taken up by the cells (a−d). Although PGHN−Dox can also be readily internalized by *S. cerevisiae* cells (e−h), PGHNs (e) and Dox (f) showed distinct distribution patterns (h). Images c and g are bright field images; images d and h are the overlaid images. The insets are enlarged images (the scale bar for the inset images is 5 $\mu$m).

## CONCLUSIONS

In summary, we have developed a new method to synthesize blue-emitting PGHNs in mild conditions. The physical and chemical properties of PGHNs were carefully evaluated using various technologies. The biocompatibility of the materials was evaluated using *E. coli* cells as a model, which suggested the low toxicity of PGHNs. The size, shape, and surface properties make these nanomaterials readily internalized by bacteria, yeast, and mammalian cells. The highly fluorescent signals from these internalized PGHNs can be readily detected by a confocal fluorescent microscope. Moreover, PGHNs can act as a nanocarrier to deliver dyes and/or drugs into cells. Therefore, we propose that PGHNs serve as a new platform in bioimaging and drug delivery studies. In addition, our research hints that small molecules such as amino acids in combination with biopolymers such as proteins can be a user-friendly way to synthesize new biocompatible biometal hybrid materials for imaging, therapeutic, and drug delivery applications.

## ASSOCIATED CONTENT

### Supporting Information

Comparison of fluorescent NPs and Trp template gold NPs, DNA gel, UV and fluorescence spectra of PGHN synthesis with different pH values, molar ratios, buffers, and capping molecules, XPS spectra, EDS map, size distribution, $\zeta$ potential, photostability, key parameters of recently reported fluorescent Au NCs/NPs and Au NPs synthesized using Trp, and additional references. This material is available free of charge via the Internet at http://pubs.acs.org.

## AUTHOR INFORMATION

### Corresponding Author

*Fax: +86 431-8519-3421. Phone: +86 186-8663-6807. E-mail: zchen@jlu.edu.cn.

### Funding

This work was supported by the National Natural Science Foundation of China (NSF) (Grant 21372097), the Open Fund of the State Key Laboratory of Reproductive Biology at the Institute of Zoology of the Chinese Academy of Sciences, and a Center of International Mobility (CIMO) grant from Finland.



DOI: 10.1021/am5083733
*ACS Appl. Mater. Interfaces* 2015, 7, 4713−4719

### Notes

The authors declare no competing financial interest.

## ■ ABBREVIATIONS

AuNCs = gold nanoclusters
NP = nanoparticle
BSA = bovine serum albumin
Trp = tryptophan
PGHNs = protein−gold hybrid nanocubes
XPS = X-ray photoelectron spectroscopy
TEM = transmission electron microscopy
SEM = scanning electron microscopy
AFM = atomic force microscopy
HEK = human embryonic kidney
Rh 6G = rhodamine 6G
Dox = doxorubicin

## ■ REFERENCES


(1) Willmann, J. K.; Bruggen, N. V.; Dinkelborg, L. M.; Gambhir, S. S. Molecular Imaging in Drug Development. *Nat. Rev. Drug Discovery* **2008**, *7*, 591−607.

(2) Murawala, P.; Tirmale, A.; Shiras, A.; Prasad, B. L. V. In Situ Synthesized BSA Capped Gold Nanoparticles: Effective Carrier of Anticancer Drug Methotrexate to MCF-7 Breast Cancer Cells. *Mater. Sci. Eng., C* **2014**, *34*, 158−167.

(3) Yong, K. T.; Law, W. C.; Hu, R.; Ye, L.; Liu, L.; Swihart, M. T.; Prasad, P. N. Nanotoxicity Assessment of Quantum Dots: from Cellular to Primate Studies. *Chem. Soc. Rev.* **2013**, *42*, 1236−1250.

(4) Li, Z.; Sun, Q.; Zhu, Y.; Tan, B.; Xu, Z. P.; Dou, S. X. Ultra-Small Fluorescent Inorganic Nanoparticles for Bioimaging. *J. Mater. Chem. B* **2014**, *2*, 2793−2818.

(5) Zhou, M. C.; Liu, B. X.; Lv, C. L.; Chen, Z. J.; Shen, J. C. Rapid Synthesis of NADPH Responsive CdSe Quantum Dots from Selenium Nanoparticles. *RSC Adv.* **2014**, *4*, 61133−61136.

(6) Jing, L. H.; Ding, K.; Kershaw, S. V.; Kempson, I. M.; Rogach, A. L.; Gao, M. Y. Magnetically Engineered Semiconductor Quantum Dots as Multimodal Imaging Probes. *Adv. Mater.* **2014**, *26*, 6367−6386.

(7) Chen, Y. C.; Zhu, C. C.; Yang, Z. H.; Chen, J. J.; He, Y. F.; Jiao, Y.; He, W. J.; Qiu, L.; Cen, J. J.; Guo, Z. J. A Ratiometric Fluorescent Probe for Rapid Detection of Hydrogen Sulfide in Mitochondria. *Angew. Chem., Int. Ed.* **2013**, *52*, 1688−1691.

(8) Guo, F. Q.; Tian, M. G.; Miao, F.; Zhang, W. J.; Song, G. F.; Liu, Y.; Yu, X. Q.; Sun, J. Z.; Wong, W. Y. Lighting up Cysteine and Homocysteine in Sequence Based on the Kinetic Difference of the Cyclization/Addition Reaction. *Org. Biomol. Chem.* **2013**, *11*, 7721−7728.

(9) Tian, M. G.; Guo, F. Q.; Sun, Y. M.; Zhang, W. J.; Miao, F.; Liu, Y.; Song, G. F.; Ho, C. L.; Yu, X. Q.; Sun, J. Z.; Wong, W. Y. A Fluorescent Probe for Intracellular Cysteine Overcoming the Interference by Glutathione. *Org. Biomol. Chem.* **2014**, *12*, 6128−6133.

(10) Eliseeva, S. V.; Bünzli, J. C. G. Lanthanide Luminescence for Functional Materials and Bio-Sciences. *Chem. Soc. Rev.* **2010**, *39*, 189−227.

(11) Pansare, V. J.; Hejazi, S.; Faenza, W. J.; Prudhomme, R. K. Review of Long-Wavelength Optical and NIR Imaging Materials: Contrast Agents, Fluorophores and Multifunctional Nano Carriers. *Chem. Mater.* **2012**, *24*, 812−827.

(12) Nel, A.; Xia, T.; Mädler, L.; Li, N. Toxic Potential of Materials at the Nanolevel. *Science* **2006**, *311*, 622−627.

(13) Casals, E.; Campos, S. V.; Bastús, N. G.; Puntes, V. Distribution and Potential Toxicity of Engineered Inorganic Nanoparticles and Carbon Nanostructures in Biological Systems. *TrAC, Trends Anal. Chem.* **2008**, *27*, 672−683.

(14) Haque, M. M.; Yeon, I. H.; Eunseo, J.; Hasan, M.; Woo, K.; Kwon, O. S. Acute Toxicity and Tissue Distribution of CdSe/CdS-MPA Quantum Dots after Repeated Intraperitoneal Injection to Mice. *J. Appl. Toxicol.* **2013**, *33*, 940−950.

(15) Chattopadhyay, P. K.; Price, D. A.; Harper, T. F.; Betts, M. R.; Yu, J.; Gostick, E.; Perfetto, S. P.; Goepfert, P.; Koup, R. A.; De. Rosa, S. C.; Bruchez, M. P.; Roederer, M. Quantum Dot Semiconductor Nanocrystals for Immunophenotyping by Polychromatic Flow Cytometry. *Nat. Med.* **2006**, *12*, 972−977.

(16) Genger, U. R.; Grabolle, M.; Jaricot, S. C.; Nitschke, R.; Nann, T. Quantum Dots versus Organic Dyes as Fluorescent Labels. *Nat. Methods* **2008**, *5*, 763−775.

(17) Xie, J.; Zheng, Y.; Ying, J. Y. Protein-Directed Synthesis of Highly Fluorescent Gold Nanoclusters. *J. Am. Chem. Soc.* **2009**, *131*, 888−889.

(18) Tan, X. H.; Jin, R. C. Ultrasmall Metal Nanoclusters for Bio-Related Applications. *Wiley Interdiscip. Rev.: Nanomed. Nanobiotechnol.* **2013**, *5*, 569−581.

(19) Zheng, J.; Nicovich, P. R.; Dickson, R. M. Highly Fluorescent Noble-Metal Quantum Dots. *Annu. Rev. Phys. Chem.* **2007**, *58*, 409−431.

(20) Zhao, Y. Y.; Tian, Y.; Cui, Y.; Liu, W. W.; Ma, W. S.; Jiang, X. Y. Small Molecule-Capped Gold Nanoparticles as Potent Antibacterial Agents That Target Gram-Negative Bacteria. *J. Am. Chem. Soc.* **2010**, *132*, 12349−12356.

(21) Zhao, Y. Y.; Jiang, X. Y. Multiple Strategies To Activate Gold Nanoparticles as Antibiotics. *Nanoscale* **2013**, *5*, 8340−8350.

(22) Ding, H.; Li, H.; Liu, P.; Hiltunen, J. K.; Wu, Y.; Chen, Z.; Shen, J. Templated In-Situ Synthesis of Gold Nanoclusters Conjugated to Drug Target Bacterial Enoyl-ACP Reductase, and Their Application to the Detection of Mercury Ions Using a Test Stripe. *Microchim. Acta* **2014**, *181*, 1029−1034.

(23) Liu, P.; Shang, L.; Li, H.; Cui, Y.; Qin, Y.; Wu, Y.; Hiltunen, J. K.; Chen, Z.; Shen, J. Synthesis of Fluorescent α-Chymotrypsin A-Functionalized Gold Nanoclusters and Their Application to Blot-Based Technology for $Hg^{2+}$ Detection. *RSC Adv.* **2014**, *4*, 31536−31543.

(24) Murawala, P.; Phadnis, S. M.; Bhonde, R. R.; Prasad, B. L. V. In Situ Synthesis of Water Dispersible Bovine Serum Albumin Capped Gold and Silver Nanoparticles and Their Cytocompatibility Studies. *Colloids Surf., B* **2009**, *73*, 224−228.

(25) Shang, L.; Nienhaus, G. U. Gold Nanoclusters as Novel Optical Probes for in Vitro and in Vivo Fluorescence Imaging. *Biophys. Rev.* **2012**, *4*, 313−322.

(26) Lee, D. E.; Koo, H.; Sun, I. C.; Ryu, J. H.; Kim, K.; Kwon, I. C. Multifunctional Nanoparticles for Multimodal Imaging and Theragnosis. *Chem. Soc. Rev.* **2012**, *41*, 2656−2672.

(27) Silva, G. A. Neuroscience Nanotechnology: Progress, Opportunities and Challenges. *Nat. Rev. Neurosci.* **2006**, *7*, 65−74.

(28) Nie, S.; Xing, Y.; Kim, G. J.; Simons, J. W. Nanotechnology Applications in Cancer. *Annu. Rev. Biomed. Eng.* **2007**, *9*, 257−288.

(29) Huang, X.; El-Sayed, I. H.; Qian, W.; El-Sayed, M. A. Cancer Cell Imaging and Photothermal Therapy in the Near-Infrared Region by Using Gold Nanorods. *J. Am. Chem. Soc.* **2006**, *128*, 2115−2120.

(30) Wu, Z. Anti-Galvanic Reduction of Thiolate-Protected Gold and Silver Nanoparticles. *Angew. Chem., Int. Ed.* **2012**, *51*, 2934−2938.

(31) Zheng, J.; Zhang, C.; Dickson, R. M. Highly Fluorescent, Water-Soluble, Size-Tunable Gold Quantum Dots. *Phys. Rev. Lett.* **2004**, *93*, 077402-1−077402-4.

(32) Mohanty, J. S.; Xavier, P. L.; Chaudhari, K.; Bootharaju, M. S.; Goswami, N.; Pal, S. K.; Pradeep, T. Luminescent, Bimetallic AuAg Alloy Quantum Clusters in Protein Templates. *Nanoscale* **2012**, *4*, 4255−4262.

(33) Wen, F.; Dong, Y.; Feng, L.; Wang, S.; Zhang, S.; Zhang, X. Horseradish Peroxidase Functionalized Fluorescent Gold Nanoclusters for Hydrogen Peroxide Sensing. *Anal. Chem.* **2011**, *83*, 1193−1196.

(34) Lin, C. A. J.; Yang, T. Y.; Lee, C. H.; Huang, S. H.; Sperling, R. A.; Zanella, M.; Li, J. K.; Shen, J. L.; Wang, H. H.; Yeh, H. I.; Parak, W. J.; Chang, W. H. Synthesis, Characterization, and Bioconjugation of Fluorescent Gold Nanoclusters toward Biological Labeling Applications. *ACS Nano* **2009**, *3*, 395−401.




DOI: 10.1021/am5083733
*ACS Appl. Mater. Interfaces* 2015, 7, 4713−4719

(35) Liu, G.; Shao, Y.; Ma, K.; Cui, Q.; Wu, F.; Xu, S. Synthesis of DNA-Templated Fluorescent Gold Nanoclusters. *Gold Bull.* **2012**, *45*, 69−74.
(36) Mu, X. Y.; Qi, L.; Dong, P.; Qiao, J.; Hou, J.; Nie, Z. X.; Ma, H. M. Facile One-Pot Synthesis of L-Proline-Stabilized Fluorescent Gold Nanoclusters and Its Application as Sensing Probes for Serum Iron. *Biosens. Bioelectron.* **2013**, *49*, 249−255.
(37) He, Q.; Shi, J. MSN Anti-Cancer Nanomedicines: Chemotherapy Enhancement, Overcoming of Drug Resistance, and Metastasis Inhibition. *Adv. Mater.* **2014**, *26*, 391−411.
(38) Ahmad, N.; Younus, H. A.; Chughtai, A. H.; Verpoort, F. Metal-Organic Molecular Cages: Applications of Biochemical Implications. *Chem. Soc. Rev.* **2015**, *44*, 9−25.
(39) Carvalho, M. A.; Shishido, S. M.; Souza, B. C.; de Paiva, R. E. F.; Gomes, A. F.; Gozzo, F. C.; Formiga, A. L. B.; Corbi, P. P. A Silver Complex with Tryptophan: Synthesis, Structural Characterization, DFT Studies and Antibacterial and Antitumor Assays in Vitro. *J. Mol. Struct.* **2013**, *1031*, 125−131.
(40) Kulesza, A.; Mitrić, R.; Koutecký, V. B.; Bellina, B.; Compagnon, I.; Broyer, M.; Antoine, R.; Dugourd, P. Doubly Charged Silver Clusters Stabilized by Tryptophan: $Ag_4^{(2+)}$ as an Optical Marker for Monitoring Particle Growth. *Angew. Chem., Int. Ed.* **2011**, *50*, 878−881.
(41) Mondal, S.; Verma, S. Catalytic and SERS Activities of Tryptophan-EDTA Capped Silver Nanoparticles. *Z. Anorg. Allg. Chem.* **2014**, *640*, 1095−1101.
(42) Maiti, N.; Thomas, S.; Jacob, J. A.; Chadha, R.; Kapoor, T. M. S. DFT and Surface-Enhanced Raman Scattering Study of Tryptophan-Silver Complex. *J. Colloid Interface Sci.* **2012**, *380*, 141−149.
(43) Satyabrata, S.; Mandal, T. K. Tryptophan-Based Peptides To Synthesize Gold and Silver Nanoparticles: A Mechanistic and Kinetic Study. *Chem.—Eur. J.* **2007**, *13*, 3160−3168.
(44) Srivastava, S. K.; Hasegawa, T.; Yamada, R.; Ogino, C.; Mizuhataa, M.; Kondo, A. Green Synthesis of Au, Pd and Au@Pd Core−Shell Nanoparticles via a Tryptophan Induced Supramolecular Interface. *RSC Adv.* **2013**, *3*, 18367−18372.
(45) Joshi, P.; Shewale, V.; Pandey, R. Tryptophan-Gold Nanoparticle Interaction: A First-Principles Quantum Mechanical Study. *J. Phys. Chem. C* **2011**, *115*, 22818−22826.
(46) Carvalho, M. A.; Shishido, S. M.; Souza, B. C.; de Paiva, R. E. F.; Gomes, A. F.; Gozzo, F. C.; Formiga, A. L. B.; Corbi, P. P. A New Platinum Complex with Tryptophan: Synthesis, Structural Characterization, DFT Studies and Biological Assays in Vitro over Human Tumorigenic Cells. *Spectrochim. Acta, A* **2014**, *122*, 209−215.
(47) Jacob, J. A.; Naumov, S.; Mukherjee, T.; Kapoor, S. Preparation, Characterization, Surface Modification and Redox Reactions of Silver Nanoparticles in the Presence of Tryptophan. *Colloids Surf., B* **2011**, *87*, 498−504.
(48) Iosin, M.; Baldeck, P.; Astilean, S. Study of Tryptophan Assisted Synthesis of Gold Nanoparticles by Combining UV-Vis, Fluorescence, and SERS Spectroscopy. *J. Nanopart. Res.* **2010**, *12*, 2843−2849.
(49) Kasture, M.; Sastry, M.; Prasad, B. L. V. Halide Ion Controlled Shape Dependent Gold Nanoparticle Synthesis with Tryptophan as Reducing Agent: Enhanced Fluorescent Properties and White Light Emission. *Chem. Phys. Lett.* **2010**, *484*, 271−275.
(50) Goldys, E. M.; Sobhan, M. A. Fluorescence of Colloidal Gold Nanoparticles Is Controlled by the Surface Adsorbate. *Adv. Funct. Mater.* **2012**, *22*, 1906−1913.
(51) Anthony, M. T.; Seah, M. P. XPS: Energy Calibration of Electron Spectrometers. 1—An Absolute, Traceable Energy Calibration and the Provision of Atomic Reference Line Energies. *Surf. Interface Anal.* **1984**, *6*, 95−106.
(52) Darrah, T. T.; Weightman, P. Valence Electronic Structure of AuZn and AuMg Alloys Derived from a New Way of Analyzing Auger-Parameter Shifts. *Phys. Rev. B* **1986**, *33*, 5406−5413.
(53) Das, S. K.; Dickinson, C.; Lafir, F.; Brougham, D. F.; Marsili, E. Synthesis, Characterization and Catalytic Activity of Gold Nanoparticles Biosynthesized with Rhizopus Oryzae Protein Extract. *Green Chem.* **2012**, *14*, 1322−1334.
(54) Cai, S. A.; Thati, S.; Bagby, T. R.; Diab, H. M.; Davies, N. M.; Cohen, M. S. Localized Doxorubicin Chemotherapy with a Biopolymeric Nanocarrier Improves Survival and Reduces Toxicity in Xenografts of Human Breast Cancer. *J. Controlled Release* **2010**, *146*, 212−218.
(55) Wang, Q. L.; Huang, X. X.; Long, Y. J.; Wang, X. L.; Zhang, H. J.; Zhu, R.; Liang, L. P.; Teng, P.; Zheng, H. Z. Hollow Luminescent Carbon Dots for Drug Delivery. *Carbon* **2013**, *59*, 192−199.


DOI: 10.1021/am5083733
*ACS Appl. Mater. Interfaces* 2015, 7, 4713−4719